One-dimensional TiO_2 nanotube array photoanode for a microfluidic all-vanadium photoelectrochemical cell toward solar energy storage

Yingying Lin[a,b#], Hao Feng[b,c#], Rong Chen[a,b]*, Biao Zhang[a,b], Liang An[d]*

[a] Key Laboratory of Low-grade Energy Utilization Technologies and Systems (Chongqing University), Ministry of Education, Chongqing 400030,China

[b] Institute of Engineering Thermophysics, School of Energy and Power Engineering, Chongqing University,Chongqing 400030, China

[c] MIIT Key Laboratory of Thermal Control of Electronic Equipment, School of Energy and Power Engineering, Nanjing University of Science & Technology, Nanjing 210094, China

[d] Department of Mechanical Engineering, The Hong Kong Polytechnic University, Hung Hom, Kowloon, Hong Kong, China

[#] Co-first authors

* Corresponding authors

[a,b] Tel.: 0086-23-65103119; fax: 0086-23-65102474; e-mail: rchen@cqu.edu.cn (Rong Chen)

[d] Tel.: 852-27667820; fax: 852-23654703; e-mail: liang.an@polyu.edu.hk (Liang An)

Abstract

In this work, a highly efficient TiO_2 nanotube array photoanode prepared by the anodizing treatment of titanium foil is developed for an all-vanadium photoelectrochemical cell with minimization design towards the solar energy storage. Such highly ordered structure presents the intrinsic advantages of not only providing large active surface area and plentiful pore volume but also enhancing the mass and electron transport. Consequently, the developed photoanode exhibits both good photoresponse and operation stability under irradiation. Besides, the solar energy storage performance of the microfluidic all-vanadium photoelectrochemical cell with

the developed TiO_2 nanotube array photoanode is evaluated under various light intensities and vanadium ion concentrations. The performances of the TiO_2 nanotube array photoanodes prepared by different anodizing voltages are also investigated. The obtained results show that the increase of both the light intensity and vanadium ion concentration can play positive roles in the performance in terms of photocurrent density and vanadium ion conversion rate. The photoanode prepared at higher anodizing voltage has larger active surface area and the photocatalyst loading, thus leading to the improved performance.

Keywords: TiO_2 nanotube array; Photoanode; All-vanadium photoelectrochemical cell; Microfluidic design; Solar energy storage

1. Introduction

Energy crisis has become one of the most concerned issues to ensure the sustainable development. For this reason, the development and utilization of renewable energy to replace the fossil fuels attract widespread attention [1-5]. Among these renewable energy sources, solar energy is the most competitive candidate because it is extensive and abundant [6-8]. However, the use of the solar energy also faces a critical issue of the intermittence. Hence, to address the inherent defect of sunlight, the storage of solar energy by converting it into the form of chemical energy is one of the most feasible approaches for the practical solar energy utilization [9, 10]. Photoelectrochemical

technology has been demonstrated to be able to convert sunlight into chemical energy through simple and efficient systems [11-13]. For example, Zhang et al. [14] proposed a photoelectrochemical system for water splitting and obtained high H_2 evolution efficiency. Li et al. [15] reduced CO_2 into methanol via photocatalytic reaction and obtained a methanol yield of 4.94 mmol L^{-1} cm^{-2} after the 6-h operation. Wang et al. [16] converted solar energy into hydrogen and electricity through a photoelectrochemical cell. Recently, Liu et al. [17] reported a method using vanadium redox pairs as the storage media to store solar energy. Among these systems, the photoelectrochemical cell using reversible redox couples of VO^{2+}, VO^{2+} and V^{3+}, V^{2+} as the storage media has been recognized as a promising scheme because of its large storage capacity, low cost and the effectiveness in avoiding cross-contamination of metal ions [18]. Hence, efforts have been devoted to the exploitation of all-vanadium photoelectrochemical cell (VPEC) [19-21].

In general, the performance improvement of the VPEC can be made via the following two strategies: the development of highly-efficient photoanode and the optimization of the cell structure [22, 23]. As the most commonly used photocatalyst, TiO_2 has been applied in numerous photoelectrochemical systems due to the remarkable merits of non-toxicity, chemical stability and low cost [24-27]. In these systems, the TiO_2 nanoparticles were usually stacked on the substrate to form the photoanode through various methods, such as wet-spraying, screen-printing, etc [28-30]. However, such stacked structure not only lowered the active surface area but also inhibited the

separation of the photo-generated electron-hole pairs, resulting in poor mass transport and photocatalytic quantum efficiency. In response to the above mentioned limitations, the photoanode with one-dimensional TiO_2 nanotube array by the anodization has been proposed [31, 32], because the one-dimensional and highly ordered nanostructure can present the intrinsic merits of facilitating the separation of photo-generated electron-hole pairs and providing large active surface area and plentiful pore volume [33, 34]. Thus, such one-dimensional structure has been considered as a favorable photoanode structure and applied in various photoelectrochemical systems [35-37].

Regarding the cell structure, the conventional H-type reactor design used in VPECs still faces the defects of both low mass transfer and large internal resistance as well as non-uniform light distribution [13, 17, 21], which significantly restricts the promotion of the solar energy storage. To address the mass transport issue, a microfluidic all-vanadium photoelectrochemical cell (μVPEC) by incorporating the microfluidic design into the VPEC has been proposed. Such combination possesses several advantages of the microfluidics, such as tremendous specific surface area and continuous-flow design [21, 24, 38], which can ensure both high mass transport efficiency and uniform light distribution and thereby present promising potential for promoting the solar energy conversion into the chemical energy [39]. However, the TiO_2 nanoparticles-stacked photoanodes used in these μVPECs still restrain the performance enhancement. Inspired by structural merits of both the microfluidic design and highly ordered one-dimensional structure, a microfluidic all-vanadium photoelectrochemical cell with a

one-dimensional TiO_2 nanotube array (TNA) photoanode was proposed for the solar energy storage in the present work. As illustrated in Fig. 1, the proposed design can offer the following desired properties to overcome the bottlenecks encountered in the conventional VPECs through the synergistic effect of the highly-ordered structure and the microfluidic design. Firstly, the one-dimensional nanotube array structure cannot only facilitate fast electron transfer but also offer large active surface area with plentiful pores, which promotes the photoelectrochemical reaction and enables high photocurrent density. Secondly, via such a microfluidic design, the transfer resistances of both the photon and reactants can be reduced. Moreover, the charge transfer resistance can be minimized. All the above-mentioned properties are in favor of enhancing the solar energy storage. In this work, the solar energy storage performance of the proposed μVPEC was evaluated under various design and operating conditions in terms of the vanadium ion conversion rate.

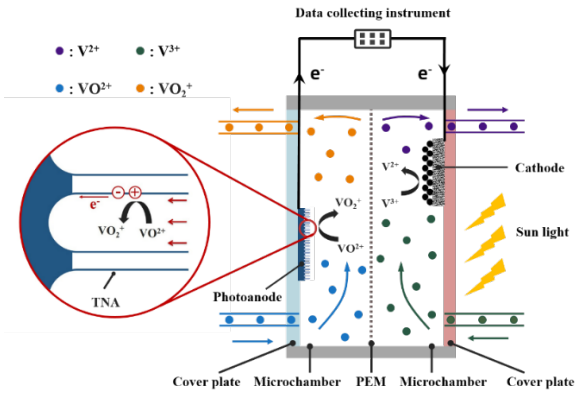

Fig. 1 Schematic illustration of the μVPEC.

2. Experimental

2.1 Preparation of the TNA photoanode

In this work, a commercial titanium foil (Xinxin Metal Plastic Materials Store, China)

with the geometry of the thickness: 0.3 mm, width: 10 mm and length: 25 mm, was used as the titanium source to prepare the photoanode through the anodization. The fabrication procedure can be described through the following three steps. Firstly, the titanium foil was placed into a mixed solution consisting of ethanol, acetone and deionized water (volume ratio = 1 : 1 : 1), and cleaned in ultrasound for 10 min to remove surface contaminants, followed by drying in the nitrogen gas stream. Secondly, the titanium foil was covered by a resin tape to obtain an electrode area of 1 cm × 1 cm in the middle region of the foil. Then, to realize the electrochemical anodization, a DC power was used. The pre-treated Ti foil and the graphite plate were directly connected to the negative and positive of the DC power, respectively, forming an applied voltage between the two electrodes in an ethylene glycol solution for 5 h. The ethylene glycol solution was prepared by dissolving NH_4F and deionized water into ethylene glycol, in which the NH_4F concentration was 0.15 M and the volume fraction of deionized water was 2%. To control the nanotube structure, the electrochemical anodization process was carried out at different DC voltages ranging from 10 V to 50 V. To remove the impurity, the obtained samples were ultrasonically cleaned in ethylene glycol for 15 min and in distilled water for 1 min, respectively. At last, to ensure the TiO_2 crystal transformation, the prepared samples were placed into a tube furnace and treated at 200 ^oC for 0.5 h and 480 ^oC for 1 h in air sequentially. Through the above-mentioned three steps, the TNA photoanode on the titanium foil was prepared successfully.

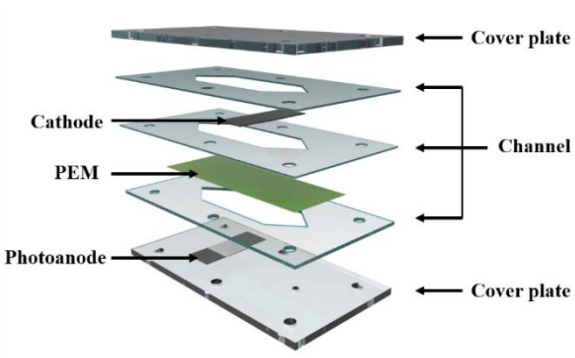

Fig. 2 Design of the μVPEC.

2.2 Assembly and setup

Fig. 2 presents the schematic description of the μVPEC. The as-synthesized TNA with the electrode area of 1 cm × 1 cm was used as the photoanode. The commercial Pt-coated carbon paper with the exposed active area of 1 cm × 1 cm was used as the cathode. Two reaction microchambers with the depth of 1 mm were used as the flow channels for the photoanode and cathode electrolytes. A Nafion®115 proton exchange membrane was used to separate the photoanode microchamber from the cathode microchamber. Both the electrolytes were injected into the μVPEC by a syringe pump. A 300 W Xe lamp was used as a simulated sunlight to illuminate the photoanode. It should be noted that the Xe lamp illuminated the photoanode from the cathode side because the TNA formed on the titanium foil was opaque. For this reason, the cell fixture was made of PMMA (Polymethyl methacrylate). Moreover, the arrangement of the photoanode and cathode was not exactly face-to-face. They were in disalignment with their minimal edge distance of 15 mm to ensure the light transmission, as illustrated in Fig. 1. Although the electrolytes at both the photoanode and cathode were translucent as a result of the existence of vanadium ions, the photons could still reach

the photoanode through the electrolyte and membrane because of narrow intervals (~ 2 mm) between the photoanode and cathode, thereby driving the anodic oxidation reaction of $VO^{2+} \rightarrow VO^{2+}$. Besides, a visible radiometer (FZ-Z, Photoelectric Instrument Factory of Beijing Normal University, China) was utilized to measure the light intensity. Real-time monitoring of the current was recorded by a data collecting instrument (34972A, Agilent, USA).

3. Results and discussion

3.1 Characterization of the photoanode

The surface topography of the prepared TNA photoanode was characterized by S-4800 field emission scanning electron microscopy (Hitachi, Japan). Fig. 3a and Fig. 3b show the top view and cross-sectional images of the prepared TNA film anodized at 50 V for 5 h. As seen, the TiO_2 nanotubes were uniformly distributed and compactly arranged on the Ti foil with the average pore size of about 82 nm. It can also be found that the mean tube length of the TNA layer was about 8.3 μm. Besides, the crystalline structure of the prepared TNA photoanode was also characterized using a D8 ADVANCE X-Ray diffractometer (Bruker, Germany) and the results are shown in Fig. 3c. As shown, the TiO_2 nanotubes were mainly composed of the anatase TiO_2 at different crystal planes, which was well consistent with previous report [40]. These results indicated the formation of the favorable one-dimensional TiO_2 nanotube array on the Ti foil. Such highly ordered structure not only provided a large active surface area but also facilitated the electron transfer through the one-dimensional structure.

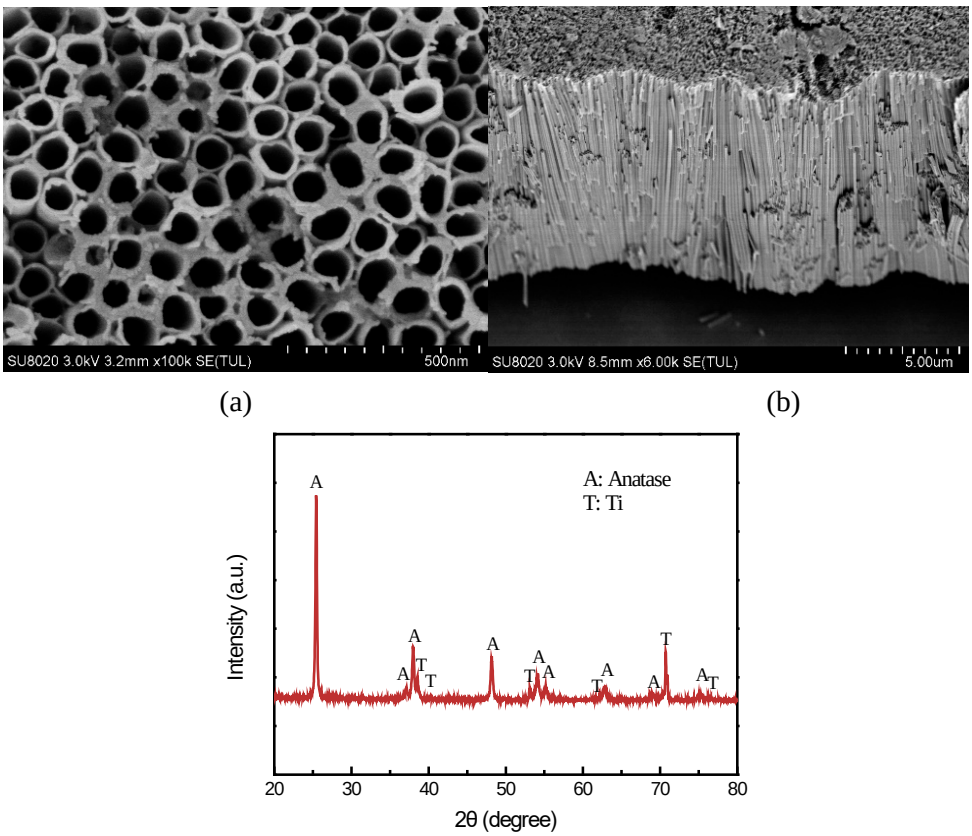

Fig. 3 (a) Top view and (b) cross-sectional view and (c) XRD spectra of the TiO_2 nanotube array (Anodizing voltage: 50 V; Anodizing time: 5 hours).

3.2 Performance evaluation

3.2.1 Photoelectrochemical activity

In general, both the photoresponse and durability under the illumination could reflect the photoelectrochemical activity of the prepared photoanode using the developed μVPEC. Hence, the photocurrent-time and the long-term operation were firstly measured to investigate the photoresponse and durability. Here, the light intensity was kept at 130 mW cm^{-2}. The photoanodic VO^{2+} and cathodic V^{3+} concentrations were both 100 mM. The flow rates of both the electrolytes were set at 50 μL min^{-1}. Fig. 4a shows the photoresponse behavior of the μVPEC with both the commonly-used P25

photoanode [21] and the developed TNA photoanode under periodic light-switch mode. It can be seen that by identifying one light-on and one light-off as a cycle, both the P25 and TNA photoanodes were able to exhibit repeatable response to the illumination in the tested five cycles. When the light was shed on the photoanode, for the TNA photoanode, the photocurrent density promptly rose to about 0.078 A g^{-1} cm^{-2} and then slightly decreased to 0.065 A g^{-1} cm^{-2} and finally became relatively stable. While for the P25 photoanode [21], the photocurrent density under the illumination was kept at about 0.025 A g^{-1} cm^{-2}, which was much smaller than that of the TNA photoanode. Besides, to describe the durability of the developed μVPEC with both the P25 and TNA photoanodes, the variation in the photocurrent density with time was also characterized, and the result is shown in Fig. 4b. It can be found that the photocurrent densities of the μVPECs with both the P25 and TNA photoanodes could be relatively stable during the 6-h operation. For the P25 photoanode, the average photocurrent density was about 0.024 A g^{-1} cm^{-2} [21]. Whereas it was boosted to 0.065A g^{-1} cm^{-2} for the TNA photoanode, presenting a remarkable improvement of about 171%, which indicated that the proposed TNA photoanode cannot only intensify the activity but also exhibit a relatively excellent stability. Such intensification of the photoelectrochemical activity can be ascribed to the synergetic effect of the highly ordered one-dimensional structure and the large active surface area with abundant pore volume. Firstly, the one-dimensional nanotube array structure could promote the electron transfer and the separation of the photo-excited electron-holes pairs [32, 33], thereby promoting the photoanode reaction. On the other hand, the nanotube array could also offer plentiful

pores and expose large active surface area, resulting in promoting the reactants transfer and providing abundant catalytic sites. Hence, compared to the traditional P25 photoanode, the photoelectrochemical activity could be significantly intensified. These results revealed that the developed TNA photoanode had good photoresponce performance and yielded a relatively stable photocurrent density for future applications.

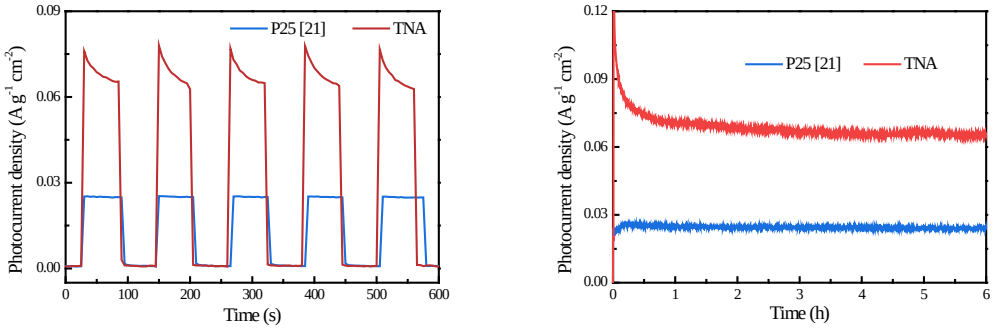

(a) (b)

Fig. 4 (a) Photoresponse behavior and (b) long-term performance of the μVPEC with the conventional P25 photoanode [21] and the proposed TNA photoanode (Light intensity: 130 mW cm^{-2}; Vanadium ion concentration: 100 mM; Flow rate: 50 μL min^{-1}).

In addition, the electrochemical impedance spectroscopy (EIS) measurement was also performed with an electrochemical workstation (CHI760E, American). In the test, the photoanode, the Ag/AgCl electrode and the platinum plate were used as the working electrode, the reference electrode and the counter electrode, respectively. The testing conditions were the light intensity of 130 mW cm^{-2} and the ion concentration of 100 mM. The tested results are given in Fig. 5. It can be seen that the charge transfer resistance of the TNA photoanode was far lower than that of the conventional P25 photoanode. This promotion can be ascribed to the highly ordered one-dimensional nanotube array structure, which not only enhanced electron transport and the separation

of the photo-excited electron-holes pairs, but also greatly increased the active sites. In addition, compared with the P25 photoanode prepared by the spraying method, the contact resistance between the nanotube array and the substrate was smaller, which also enhanced the electron transfer. Therefore, the TiO_2 nanotube array photoanode possessed smaller impedance, leading to the improved performance.

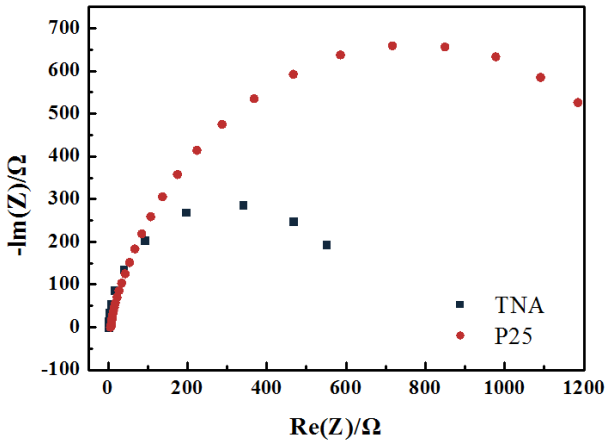

Fig. 5 EIS Nyquist plots of the TNA and P25 photoanodes.

3.2.2 Conversion rate of the vanadium ions

To more clearly present the inherent merits of the μVPEC with the TNA photoanode, the performance of the solar energy conversion was also discussed under various operation conditions via the conversion rate of VO^{2+} to VO_2^+. In the present study, the vanadium ion conversion rate, N (μmol/h), was evaluated using the following equations:

$$Q = \int_0^T I dt \quad (1)$$

$$N = Q/(T \cdot F) \quad (2)$$

where Q (C), I (A), T (h) and F represent the total charge during the operation period, the photocurrent, the operation time and the Faraday's constant. Basically, the solar

energy storage via the change of the valence states of the vanadium redox couples can proceed essentially once the light is irradiated on the photoanode. Therefore, the light intensity could act as a significant role in affecting the solar energy storage performance. Fig. 6a shows the effect of the light intensity on the conversion rate. During the testing, the V^{3+} and VO^{2+}concentrations of 100 mM, and the photoanodic and cathodic flow rates of 50 μL min^{-1} were chosen. As shown, when the light intensity was set at 70 mW cm^{-2}, the conversion rate was only 0.97 μmol h^{-1}. However, as the light intensity increased from 70 to 130 mW cm^{-2}, it was remarkably intensified to 2.14 μmol h^{-1}. Such intensification could be ascribed to the following reasons. On one hand, the increase of light intensity indicated that more photons reached the photoanode, which allowed for more electron-hole pairs to be generated and thus produced more photo-excited holes with strong oxidability to convert VO^{2+} into VO_2^+. On the other hand, the increased light intensity could provide more photons to generate more photo-excited electrons, which may recombine with the holes more frequently and thus inhibit the vanadium ion conversion. However, benefited from the intrinsic merit of the one-dimensional TiO_2 nanotube structure that facilitates the electron transfer, the recombination of the photo-generated electrons and holes can be restrained to some extent, leading to the intensification of the solar energy conversion.

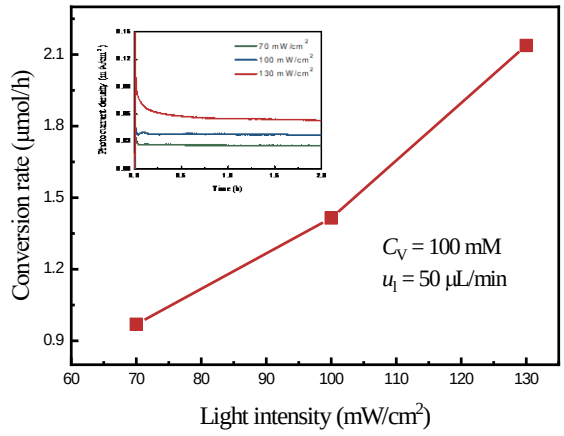

(a)

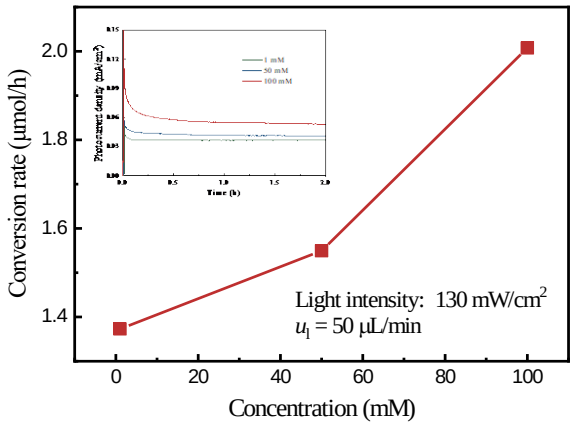

(b)

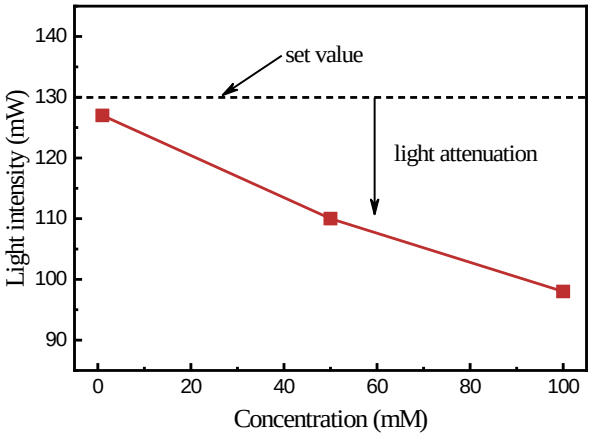

(c)

Fig. 6 Variations of the conversion rate with (a) the light intensity and (b) vanadium ion concentration, and (c) the change of the light attenuation with the vanadium ion concentration.

In addition, the influence of the vanadium ion concentration on the solar energy conversion were also studied. In this part, the light intensity of 130 mW cm^{-2} and the

electrolytes flow rates of 50 μL min^{-1} were used. To balance the charges in the photoanodic and cathodic microchambers, the vanadium ion concentrations at both the electrodes were kept the same and changed simultaneously. The vanadium ion concentrations of the electrolytes ranged from 1 mM to 100 mM. Fig. 6b shows the effect of the vanadium ion concentration on the conversion rate. As seen, the conversion rate was gradually intensified from 1.459 μmol h^{-1} to 1.983 μmol h^{-1} with the increase of the vanadium ion concentration, indicating that the increased concentration can play a positive effect on the photoelectrochemical reaction. The increased vanadium ion concentration can reduce the mass transfer resistance from the bulk to the active sites. The enhanced mass transfer means that the photo-excited holes can be captured by VO^{2+} more efficiently, accelerating the separation of the electron-hole pairs. Hence, the reaction rate at the TNA photoanode could be intensified to enlarge the photocurrent density, leading to the improvement in solar energy conversion. Specially, it can also be found that the increasing trend of the conversion rate from 1 mM to 50 mM was smaller than that from 50 mM to 100 mM. Such disparity could be attributed to the combined effect of the mass transfer enhancement and the light attenuation deterioration through the photoanodic and cathodic electrolytes caused by the increased concentration. As shown in Fig. 6c, with the increased concentration, the light attenuation through the electrolytes became increasingly distinct. Actually, the light attenuation and the increase of the vanadium ion concentration play the opposite roles in the performance. As discussed above, the light intensity can significantly influence the solar energy conversion. The more light attenuation indicated that the photon

irradiation on the TNA photoanode was inhibited. Whereas for the increase of the vanadium ion concentration, the enhanced ion transfer can result in the capture of the photo-excited holes to be more efficient. Hence, when increasing the vanadium ion concentration, the competition between the light attenuation and the intensification of the ion transfer determines the cell performance. As the concentration increased from the 1 mM to 50 mM, the light intensity declined from 127 mW cm^{-2} to 110 mW cm^{-2}, displaying an adverse effect on the vanadium ion conversion. However, due to the positive contribution from the enhanced mass transfer, smaller enhancement of the ion conversion rate could still be achieved. While for the further increase of the ion concentration to 100 mM, the light intensity irradiated on the photoanode surface was reduced to 98 mW cm^{-2}. Although the deteriorated light attenuation further restricted the photoelectrochemical reaction, the increased concentration can more significantly contribute to the performance improvement, resulting in more significant promotion of the conversion rate.

Table 1 Performance comparison between the present study and previous works.

Cell design	Catalyst	Catalyst loading (mg)	C_v (mM)	I_d (mA cm^{-2})	I (mA cm^{-2} mg^{-1})	Ref.
H-type	CCT	-	10	~0.027	-	[41]
H-type	TNB	-	10	~0.029	-	[19]
μVPEC	P25 TiO_2	3	100	0.073	0.024	[21]
μVPEC	TNT	1	100	0.035	0.035	[39]
μVPEC	TNA	0.78	100	0.051	0.065	This work

Abbreviations: C_v, Vanadium ion concentration; I_d, photocurrent per unit surface area; I, photocurrent per unit surface area and catalyst loading; TNB, TiO_2 nanobelts; CCT, carbon coated TiO_2 nanoparticle; TNT, multi-nanostructured TiO_2.

To further demonstrate the merits of the μVPEC with the TNA photoanode, we also made a performance comparison with the reported studies, as listed in Table 1. As can be seen, in terms of the reactor structure, the performance of the μVPEC was higher than that of the conventional H-type batch reactor as a result of enhanced mass and photon transport and more uniform light distribution arising from the microfluidic design. With regard to the photocatalyst type, the one-dimensional TNA exhibited better performance than did those photoanodes with the nanoparticles stacked on the substrates as a result of enhanced electron transfer. In particular, benefited from the combination of the microfluidic reactor and TiO_2 nanotube arrays, the photocurrent density were larger than the other designs. These results indicate that the μVPEC with the TNA photoanode exhibits good photoelectrochemical activity and shows outstanding potential for future applications in solar energy storage.

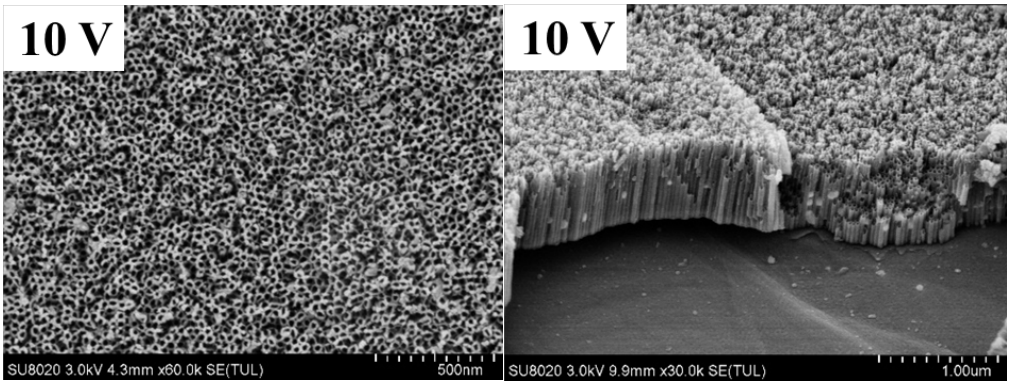

(a) (b)

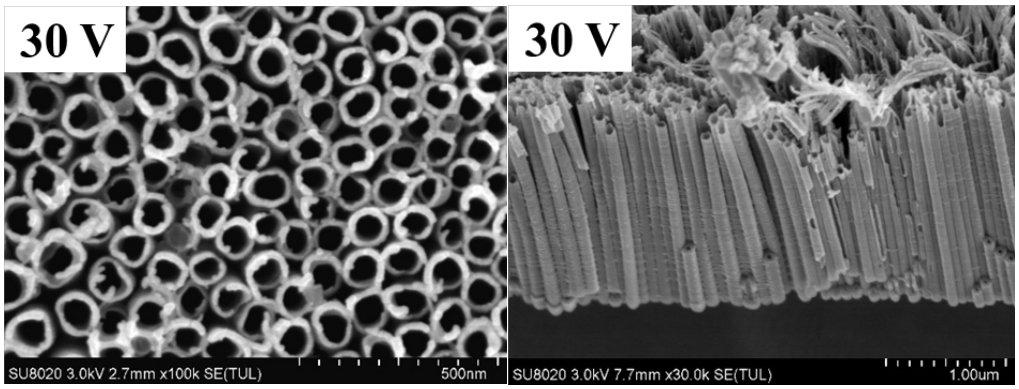

(c) (d)

Fig. 7 Top view and cross-sectional views of the TiO_2 nanotube arrays prepared under different anodizing voltages of 10 V (a, b) and 30 V (c, d).

3.3 Effect of the anodizing voltage

Since the nanostructure of the anodized TiO_2 nanotube array strongly depends on the anodizing voltage, the influence of the anodizing voltage on the performance was discussed in this section. Three sampling photoanodes prepared under the anodizing voltages of 10 V, 30 V and 50 V were chosen and investigated. The top views and cross-sectional views of the prepared TNA photoanodes under different anodizing voltages are given in Fig. 7. By comparing the results in Figs. 3a, 3b and 7, it can be found that with the increase of the anodizing voltage from 10 V to 50 V, the average pore size of the nanotube was gradually enlarged from about 18 nm to about 82 nm. The mean nanotube length was increased from about 0.6 μm to 8.3 μm, and the pore density was decreased from about 53.47×10^9 pores cm^{-2} to 9.83×10^9 pores cm^{-2}. In addition, to further describe the disparity of the TNA samples prepared under different anodizing voltages, according to previous studies [42-44], the exposed surface area and specific surface area were also calculated using the following equations:

$$A_i = \frac{1}{4}\pi(D_0^2 - D_i^2) + \pi L(D_0 + D_i) \quad (3)$$

$$A_0 = \frac{nA_i}{10^{14}} \quad (4)$$

where D_i (nm) and D_0 (nm) denote the average inner and outer diameter of nanotubes; A_i (nm^2 per tube) represents the exposed surface area of single nanotube; L (nm) is the mean tube length of nanotubes; A_0 (cm^2 cm^{-2}) is the exposed surface area per unit electrode area, which was 1 cm × 1cm in this work; n (pores cm^{-2}) is the pore density, which means the total number of pores in unit TNA area.

Besides, the photocatalyst loading could be determined by the following equation:

$$M = \rho V \quad (5)$$

where M (mg cm^{-2}) is the TNA loading; ρ is the density of anatase TiO_2, i.e. 3.85 g cm^{-3}, because the TiO_2 nanotubes were mainly composed of the anatase TiO_2 (see Fig. 3c and Fig. 8); V (cm^3) is the total volume of the prepared TNA photocatalyst. In this work, the total volume of TNA, V, was estimated by:

$$V = nLSA \quad (6)$$

where L (nm) is the mean tube length of nanotubes and determined by the cross-sectional SEM images of the TNA samples; S (cm^2) is the top area of single nanotube; A is the electrode area, i.e. 1 cm × 1 cm = 1 cm^2. The top area, S, is calculated by the equation (7):

$$S = \frac{\pi(D_o^2 - D_i^2)}{4 \times 10^{14}} \quad (7)$$

With these equations, the photocatalyst loading could then be estimated and given in Table 2.

Table 2 Variations of the TNA properties with the anodizing voltage.

Anodizing voltage (V)	D_i (nm)	D_o (nm)	L (μm)	n (pores/cm^2)×10^9	A_0 (cm^2 cm^{-2})	M (mg cm^{-2})
10	18.01 ± 1.72	48.17 ± 3.39	0.63 ± 0.02	53.47	70.36±4.05	0.20± 0.03
30	54.68 ± 2.75	85.97 ± 1.77	1.66 ± 0.05	10.19	74.84±1.93	0.22± 0.02
50	82.02 ± 1.75	99.40 ± 1.12	8.29 ± 0.24	9.83	464.35±12.05	0.78± 0.10

Table 2 lists the detailed information of the pore density and the exposed surface area as well as the specific surface area of the samples prepared under various anodizing voltages. As can be seen, benefited from smaller pore size, the TNA sample prepared under low anodizing voltage can show the larger pore density. Low anodizing voltage also resulted in the shorter nanotube length. Although the pore density was gradually declined with increasing the voltage, the enlarged mean nanotube length led to the increase of both the exposed surface area and the TNA photocatalyst loading. As such, the exposed surface area per unit electrode area was remarkably intensified from 70.36 cm^2/cm^2 (10 V) to 464.35 cm^2/cm^2 (50 V). The photocatalyst loading increased from 0.20 mg cm^{-2} at 10 V to 0.78 mg cm^{-2} at 50 V (see Table 2). The increase of both the exposed surface area and photocatalyst loading can provide more active sites for the photoelectrochemical reaction, thus having the potential to enhance the performance.

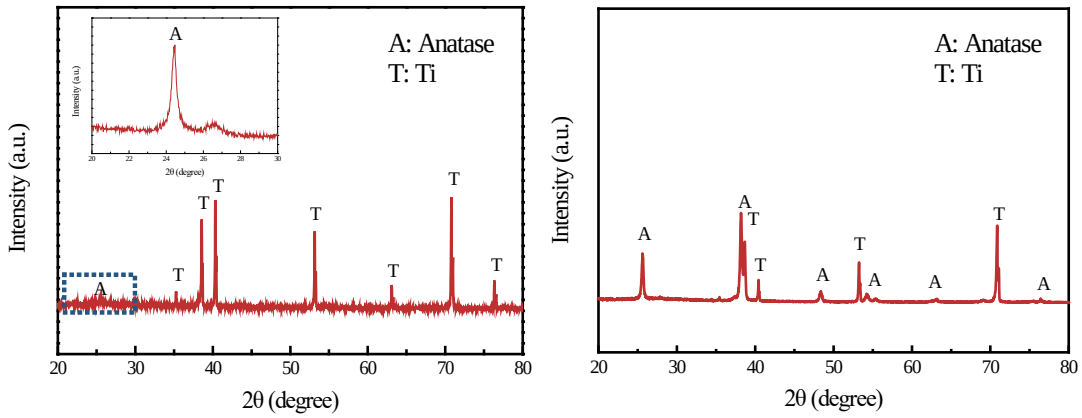

(a) (b)

Fig. 8 XRD spectra of the prepared TNA samples at the anodizing voltages of (a) 10 V and (b) 30 V.

Furthermore, the crystalline structures of the above-mentioned samples were also characterized using XRD, and the results are shown in Fig. 8. As shown, the XRD peaks of anatase TiO_2 and Ti substrate can be observed for all of these three samples, whereas the intensity of the TiO_2 signal was gradually enhanced with the increased anodizing voltage (see Figs. 3c and 8). This is because at low anodizing voltage of 10 V, only a thin TNA layer could be formed on the Ti foil (see Fig. 7a), the intensity of Ti substrate signal thus represents more remarkable. Whereas with the increase of the anodizing voltage, both the mean nanotube length and the TNA loading were increased (see Fig. 7b and Table 2), resulting in obviously increased intensity of TiO_2 signal.

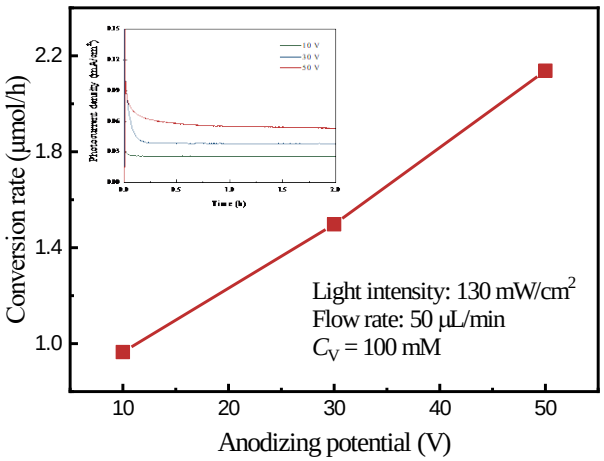

Fig. 9 Effect of the anodizing voltage on the photocurrent density and the vanadium ion conversion rate.

At last, the performance of the TNA photoanodes prepared under different anodizing voltages were assessed and the results are shown in Fig. 9. Here, the light intensity of 130 mW cm^{-2}, the ion concentrations of 100 mM and the flow rates of 50 μL min^{-1} at both the photoanode and cathode, respectively, were selected. As shown in Fig. 9, the conversion rate of the vanadium ion was intensified from 0.97 μmol h^{-1} to 2.14 μmol h^{-1} with increasing the anodizing voltage from 10 V to 50 V. As discussed above, with the increase of the anodizing voltage, both the exposed surface area and photocatalyst loading were increased. Because the increased active surface area and TNA loading could offer more active sites for the photoelectrochemical reaction, more VO^{2+} could be oxidized on the TNA surface of the photoanode. Meanwhile, with the increase of the anodizing voltage, the larger pore size of the TiO_2 nanotube could facilitate the transport of the vanadium ions into the nanotubes [44], which could also increase the photoelectrochemical reaction rate by smoothing the adsorption and desorption on the catalyst surface, leading to the improved solar energy storage.

4. Conclusions

In this work, a high-performance photoanode with the one-dimensional TiO_2 nanotube array was developed for a microfluidic all-vanadium photoelectrochemical cell to efficiently store solar energy. By combining the merits of the miniaturization design and the one-dimensional nanotube structure, the proposed μVPEC can provide the reinforced advantages of large active surface area and abundant pores in accompany with fast electron transfer, resulting in higher energy conversion efficiency. The experimental results indicated that the proposed TNA photoanode could yield good photoresponse and stability towards the illumination. Besides, the effects of both the light intensity and the concentration of the vanadium ion as well as the anodizing voltage were also studied. It can be found that the intensification of both the light intensity and vanadium ion concentration facilitated the improvement in both the photocurrent density and vanadium ion conversion rate because more electron-hole pairs were generated and the mass transport was enhanced, respectively. High anodizing voltage could result in the TNA with larger active surface area and photocatalyst loading, leading to more efficient solar energy storage. Furthermore, it should also be pointed out that although proposed photoanode in accompany with the microfluidic design can significantly intensify the photocurrent, the output of the μVPEC is still rather small. More works on the integration of multiple microreactors and the optimization of the photoanode may be necessary to distinctly improve the overall output of the system for real applications.

Acknowledgments

The authors gratefully acknowledge the financial supports of the National Natural Science Foundation of China (No. 51925601), the Program for Back-up Talent Development of Chongqing University (No. CQU2017HBRC1A01), the Fundamental Research Funds for the Central Universities (No. 2018CDXYDL0001) and the Research Grants Council of the Hong Kong Special Administrative Region, China (No. 25211817).

References

[1] Y. Chisti, Biotechnol. Adv., 2007, 25, 294-306.

[2] P. M. Schenk, S. R. Thomas-Hall, E. Stephens, U. C. Marx, J. H. Mussgnug, C. Posten, O. Kruse and B. Hankamer, BioEnerg. Res., 2008, 1, 20-43.

[3] Q. Liao, X. Zhu, X. Y. Zheng and Y. D. Ding, J. Power Sources, 2007, 171, 644-651.

[4] R. Wu, Q. Liao, X. Zhu and H. Wang, Int. J. Heat Mass Transf., 2011, 54, 4341-4348.

[5] X. Zhu, Q. Liao, P.C. Sui and N. Djilali, J. Power Sources, 2010, 195, 801-812.

[6] N.S. Lewis, Science, 2007, 315, 798-801.

[7] J. Burschka, N. Pellet, S. J. Moon, R. Humphry-Baker, P. Gao, M. K. Nazeeruddin and M. Grätzel, Nature, 2013, 499, 316-319.

[8] B. O'Regan and M. Grätzel, Nature, 1991, 353, 737-740.

[9] M. M. Lee, J. Teuscher, T. Miyasaka, T. N. Murakami and H. J. Snaith, Science, 2012, 338, 643-647.

[10] S. Linic, P. Christopher and D. B. Ingram, Nat. Mater., 2011, 10, 911-921.

[11] S. Mahzoon, S. M. Nowee and M. Haghighi, Renew. Energ., 2018, 127, 433-443.

[12] S. Xie, Q. Zhang, G. Liu and Y. Wang, Chem. Commun., 2016, 52, 35-59.

[13] Y. Shen, Z. Wei, D. Liu, H. Almakrami and F. Liu, Mater. Res. Bull., 2017, 96, 431-436.

[14] X. Y. Zhang, H. P. Li, X. L. Cui and Y. H. Lin, J. Mater. Chem., 2010, 20, 2801-2806.

[15] P. Li, H. Jing, J. Xu, C. Wu, H. Peng, J. Lu and F. Lu, Nanoscale, 2014, 6, 11380-11386.

[16] Z. Wang, Y. Lin, R. Chen, Q. Liao, X. Zhu, L. An, X. He and W. Zhang, Electrochim. Acta, 2017, 245, 549-560.

[17] D. Liu, Z. Wei, C. J. Hsu, Y. Shen and F. Liu, Electrochim. Acta, 2014, 136, 435-441.

[18] Z. Wei, D. Liu, C. Hsu and F. Liu, Electrochem. Commun., 2014, 45, 79-82.

[19] Z. Wei, Y. Shen, D. Liu, C. Hsu, S. D. Sajjad, K. Rajeshwar and F. Liu, Nano Energy, 2016, 26, 200-207.

[20] D. Liu, W. Zi, S.D. Sajjad, C. Hsu, Y. Shen, M. Wei and F. Liu, ACS Catal., 2015, 5, 2632-2639.

[21] X. Jiao, R. Chen, X. Zhu, Q. Liao, D. Ye, B. Zhang, L. An, H. Feng and W. Zhang,

Electrochim. Acta, 2017, 258, 842-849.

[22] M. Chen, R. Chen, X. Zhu, Q. Liao, L. An, D. Ye, Y. Zhou, X. He and W. Zhang, J. Power Sources, 2017, 371, 96-105.

[23] L. Li, R. Chen, X. Zhu, Q. Liao, H. Wang, L. An and M. Zhang, J. Catal., 2016, 344, 411-419.

[24] L. Li, G. Wang, R. Chen, X. Zhu, H. Wang, Q. Liao and Y. Yu, Lab Chip, 2014, 14, 3368-3375.

[25] L. Li, R. Chen, X. Zhu, H. Wang, Y. Wang, Q. Liao and D. Wang, ACS Appl. Mater. Inter., 2013, 5, 12548-12553.

[26] S. Moghaddam, M. M. Zerafat and S. Sabbaghi, Int. J. Nano Dimens., 2018, 9, 89-103.

[27] H. Feng, X. Jiao, R. Chen, X. Zhu, Q. Liao, D. Ye, B. Zhang and W. Zhang, J. Power Sources, 2019, 419, 162-170.

[28] Y. Kameya, H. Yamaki, R. Ono and M. Motosuke, Mater. Lett., 2016, 175, 262-265.

[29] L. Li, S. Xue, R. Chen, Q. Liao, X. Zhu, Z. Wang, X. He, H. Feng and X. Cheng, Electrochim. Acta, 2015, 182, 280-288.

[30] S.R. Adawiyah and Endarko, International Symposium on Current Progress in Functional Materials, 2017, 188, 012062.

[31] G. K. Mor, O. K. Varghese, M. Paulose, K. Shankar and C. A. Grimes, Sol. Energ. Mater. Sol. C., 2006, 90, 2011-2075.

[32] S .A. Yavari, Y. C. Chai, A. J. Böttger, R. Wauthle, J. Schrooten, H. Weinans and

A. A. Zadpoor, Mater. Sci. Eng. C, 2015, 51, 132-138.

[33] L. J. Li, Z. Q. Zhou, J. L. Lei, J. X. He, S. T. Zhang and F. S. Pan, Appl. Surf. Sci., 2012, 258, 3647-3651.

[34] H. Wang, H. Y. Li, J. S. Wang, J. S. Wu, D. S. Li, M. Liu and P. L. Su, Electrochim. Acta, 2014, 137, 744-750.

[35] W. B. Huang, X. Y. Wang, Y. L. Xue, Y. Yang and X. Y. Ao, RSC Adv., 2015, 5, 56098-56102.

[36] Y. Yao, K. Li, S. Chen, J. Jia, Y. Wang and H. Wang, Chem. Eng. J., 2012, 187, 29-35.

[37] M. Zhang, J. Cheng, X. X. Xuan, J. H. Zhou and K. F. Cen, ACS Sustain. Chem. Eng., 2016, 4, 6344-6354.

[38] H. Feng, X. Zhu, R. Chen, Q. Liao, J. Liu and L. Li, Chem. Eng. J., 2016, 306, 1017-1025.

[39] H. Feng, X. Jiao, R. Chen, X. Zhu, Q. Liao, D. Ye and B. Zhang, J. Power Sources, 2018, 404, 1-6.

[40] Z. Liu, X. Zhang, S. Nishimoto, M. Jin, D. A. Tryk, T. Murakami and A. Fujishima, J. Phys. Chem. C, 2008, 112, 253-259.

[41] Z. Wei, D. Liu, Y. Shen, H. Chia-Jen and F. Liu, ECS Transactions, 2015, 66, 213-221.

[42] S. A. A. Yahia, L. Hamadou, A. Kadri, N. Benbrahim and E. Sutter, J. Electrochem. Soc., 2012, 159, K83-K92.

[43] P. Xiao, B. B. Garcia, Q. Guo, D. Liu and G. Cao, Electrochem. Commun., 2007,

9, 2441-2447.

[44] K. C. Sun, Y. C. Chen, M. Y. Kuo, H. W. Wang, Y. F. Lu, J. C. Chung, Y. C. Liu and Y. Z. Zeng, Mater. Chem. Phys., 2011, 129, 35-39.